RESEARCH ARTICLE | JANUARY 13 2017

Diffraction radiation based on an anti-symmetry structure of spoof surface-plasmon waveguide

Jun Jun Xu ; Xing Jiang; Hao Chi Zhang ; Jiafu Wang; Shaobo Qu; Tie Jun Cui

Appl. Phys. Lett. 110, 021118 (2017)
https://doi.org/10.1063/1.4974148

Diffraction radiation based on an anti-symmetry structure of spoof surface-plasmon waveguide

Jun Jun Xu,[1,2,3] Xing Jiang,[2] Hao Chi Zhang,[1,3] Jiafu Wang,[4] Shaobo Qu,[4] and Tie Jun Cui[1,3,a)]
[1]*State Key Laboratory of Millimeter Waves, Southeast University, Nanjing 210096, China*
[2]*Guangxi Colleges and Universities Key Laboratory of Microwave and Optical Wave-applied Technology, Guilin, 541004, China*
[3]*Synergetic Innovation Center of Wireless Communication Technology, Nanjing, 210096, China*
[4]*College of Science, Air Force Engineering University, Xi'an, Shaanxi 710051, China*

(Received 14 November 2016; accepted 4 January 2017; published online 13 January 2017)

Spoof surface-plasmon (SP) modes can be excited efficiently and propagate along the surface of double-layer corrugated metallic strips with anti-symmetry. Here, we propose a spoof SP structure with diffraction radiation, which is achieved by introducing phase-reversal geometry into the SP waveguide structure with a π-phase shift for adjacently reversed units. At the junction between two adjacent units, the discontinuity of the periodic structure can be viewed as a perturbation to generate space harmonics, thereby enabling efficient conversion of SP modes into free-space radiation modes. We demonstrate experimentally that the resultant radiation is analogous to Cherenkov radiation wakes, which occurs in the form of a radiation cone. The vast majority of the energy based on the surface wave is emitted into the free space. We expect that the proposed method could be an alternative to transforming the spoof SP modes into the radiation modes. *Published by AIP Publishing.*
[http://dx.doi.org/10.1063/1.4974148]

Charged particles, such as electrons, emit radiations when passing through a dielectric medium if the velocity of particles exceeds the phase velocity of light in the dielectric medium. This effect, known as Cherenkov radiation, was first observed by Cherenkov and Vavilov and theoretically interpreted by Tamn and Frank in the 1930s.[1] In plasmonic Cherenkov radiation,[2,3] similar to the traditional Cherenkov radiation, the Cherenkov angle (i.e., the semiangle of the Cherenkov cone) is determined by the ratio of the two speeds. Recent research on plasmonic Cherenkov radiations has been mainly focused on the excitation of a swift electromagnetic (EM) source moving on the interface of semiconductors[4] and metals.[5] In Ref. 6, backward Cherenkov radiation was experimentally observed in negative-index metamaterials, whereas in Refs. 7 and 8, a Cherenkov phase-matching scheme was used to generate a broadband terahertz source, which can effectively improve the efficiency of the terahertz generation.

Cherenkov radiation is typically described in terms of particle radiation but essentially is the same phenomenon as the leaky-wave radiation due to the wave-particle duality. In both Cherenkov and leaky-wave cases, the radiation wakes in the form of a cone with half angle are determined by the ratio of the two speeds. If the electron velocity exceeds the phase velocity of light in the dielectric medium, the surface wave will be coupled to radiation modes in the transmission line. Cherenkov radiation wakes can be attained by the introduction of a periodic structure with a longitudinal period. For instance, a line-envelope tilted nanoslit array has been used for tuning the surface-plasmon (SP) excitation characteristics.[9] When particles traveling near a metallic structure, particularly metallic grating or an array of nanoslits, the phase velocity can be altered dramatically by employing a periodic medium, and in that case, one can even achieve the Cherenkov radiation with no minimum particle velocity—a phenomenon known as the Smith-Purcell effect, which is treated as the resonant diffraction radiation.[10–13]

Recent research has indicated that the subwavelength metal-array structures strongly support the transmission of surface waves.[14,15] The interaction between the conduction electrons of the metal and surrounding electromagnetic (EM) field can generate surface-wave modes, known as surface plasmon polaritons (SPPs), which are two-dimensional (2D) EM fields. These modes are characterized by a propagating or localized behavior, leading to a variety of unique physical phenomena, particularly the advantages of subwavelength-scale confinements and manipulations of light. The enhanced and localized fields can be harnessed to increase the sensitivity and performance of numerous physical phenomena and applications.

However, SPPs cannot be excited effectively in the lower frequency band since the metal shows a perfect electric conductor (PEC) property in microwave and terahertz frequencies. To overcome this problem, patterning the surface with subwavelength periodic features can be viewed as surface defects, which modify the surface morphology, mimicking the SPP properties in the optical frequency and leading to "spoof" SPPs with subwavelength confinements at much lower frequencies. An ultrathin corrugated metallic strip, as a typical 2D SPP transmission line in the microwave regime, has recently emerged as a new research branch in photonics that has attracted substantial research efforts.[16,17] Such a spoof surface plasmonic waveguide can strongly support SPP-like surface modes along the surface of the metal, usually referred to as spoof-plasmons, solving the problem that SPPs cannot be excited efficiently on flat metallic surfaces.

a)Email: tjcui@seu.edu.cn

Due to the mismatch of momentum between SPPs and spatial propagating modes, the excited SPPs are confined on the structured metal surface, which are impossible to be converted to spatial waves directly. Gradient-index metasurfaces offer a new paradigm for manipulation of SPP traveling in the vicinity of the surface.[18–20] For example, Ni *et al.* adopted a "V-shaped" plasmonic metasurface,[21] introducing a constant phase shift between two neighbor units, which diffracts the EM waves to the far field at a specific radiation angle with a small angular divergence.[22,23] The manipulation of the phase of the reflection coefficient plays a fundamental role in generating synthetic scattering diagrams of macroscopic objects.[24,25] Hence, plasmonic metasurface can also serve as a radiation source, enhancing and shaping the spectral and spatial distributions of the emitted radiations.

In this letter, we propose a method to efficiently generate 2D diffraction radiation. We propose a structure based on the highly localized transmission line, which is composed of two ultrathin corrugated metallic strips printed on the top and bottom surfaces of a dielectric substrate with the antisymmetry.[26,27] The fundamental mode (TM mode) of the corrugated transmission line does not radiate since the electric field is strongly bounded between the two metallic lines. The structure presents an abrupt discontinuity when introducing the periodic phase-reversal geometry, which can excite the higher-order modes and lead to leakages.[28,29] The reversed symmetric coupling structure clearly has an effect to reduce the size of the device. Experiments in the microwave region, including both dispersion and near-field characterizations, are in excellent agreements with the numerical results. Once the surface waves can be effectively transformed to radiation modes, it would pave the way for the generation of SP radiation sources.

Figure 1 illustrates the proposed structure and shows the cross section of the geometry, which can be regarded as a series-fed array. Two identical patterned metallic strips on both sides of the substrate are arranged in mirror symmetry with respect to the reference plane (i.e., the XOZ plane), resulting in two coupled single-side strips with opposite corrugation orientations. The structure is based on the parallel coupled line, which is composed of a plurality of parallel transmission line segments periodically interconnected by matching stub with width of d. The two types of transmission line segments are illustrated in Figure 1(a), which are composed of the top and bottom metallic surfaces alternately, with a strip length $l/2$ and different offset g. The matching stub is formed with a bridge in connection between the two pairs. Since the coupling coefficient depends on the horizontal distance (g) between the parallel lines on the upper and lower layers, the transmission line segments will form different characteristic impedances, Z_{01} and Z_{02}, as shown in Fig. 1(b), which will introduce an impedance discontinuity. Therefore, the connecting wire is usually with the length of a quarter wavelength for impedance transformation, which can effectively suppress local reflections. As a result, this configuration can be considered as two half-wavelength-long lines connected in tandem via a matching transmission line of quarter-wavelength long.

Without the introduction of periodic phase-reversal geometry, the structure is merely a uniform spoof SP waveguide,

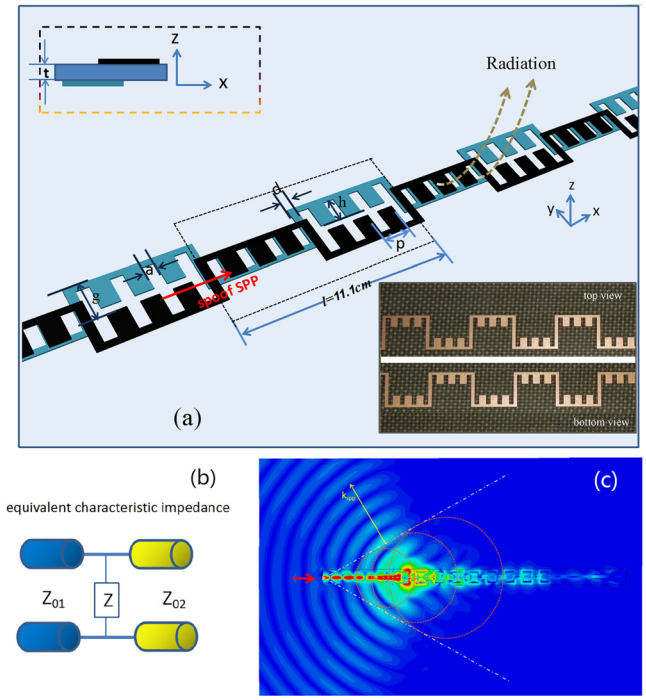

FIG. 1. (a) Schematic view of the proposed structure for the analogue of Cherenkov radiation wakes. The structure is composed of a plurality of balanced transmission line segments periodically interconnected by matching stub with a period of l. The dielectric substrate is Rogers RT5880 with a dielectric constant of 2.65 and thickness t = 0.17 mm. Here, the layout parameters are as follows: a = 0.6 mm, d = 0.45 mm, and p = 1.5 mm. The inset shows the photograph of the fabricated phase-reversal structure. (b) The equivalent characteristic impedance of the unit cell (see the dashed box in (a) for the unit cell). (c) Excitation of Cherenkov radiation wakes in the spoof SP waveguide. The radiation wakes is the result of the superposition of the radiation from each point of the trajectory.

which is constructed by arranging mirror duplicated unit cells periodically along the x-axis. Due to the strong EM coupling between such double-corrugated metallic strips, the excited SP mode has been demonstrated with higher confinements and less crosstalk properties compared with conventional microstrip lines.

The spoof SP mode can be highly localized on the structured metal surface, which exhibits a slow-wave dispersion behavior and excellent transmission performance, as shown by the blue dotted line in Fig. 2. It is a purely guiding (nonradiative) slow-wave structure. The phase-reversal geometry transforms the structure into a periodic discontinuous structure.

The coupled corrugated geometry bears some resemblance in its topology. In order to understand the physical mechanism for introducing the phase-reversal structure, we first compare the dispersion characteristics of the corrugated strip, as illustrated in Figure 2. We set periodic boundary conditions for the unit cell to calculate the dispersion relation by using the Eigenmode Solver in the commercial software, CST Microwave Studio. The dispersion curves are sensitive to the offset (g) between the two metal layers along the Y direction. When increasing the offset (g) along the Y direction, EM fields are still confined as before, starting from the origin ($k_0 = \beta = 0$) of the dispersion diagram, with only a slight increase in the cutoff frequency. The black line is the light line, i.e., $k_0 = w\sqrt{\varepsilon_0\mu_0}$, where k_0 is the free-space wave number. When the offset (g) between the upper and lower

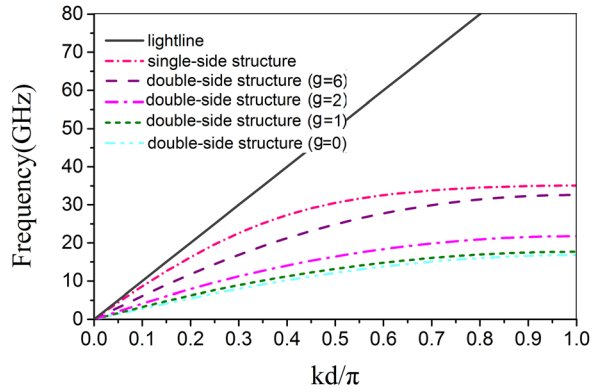

FIG. 2. The dispersion relations of the corrugated metallic strip unit for different offsets (g), obtained via CST eigenmode simulations. When the offset (g) between the upper and lower layers ranges from 6 mm to 0, it will result in the corresponding dispersion curves gradually deviated from the light line (the black line).

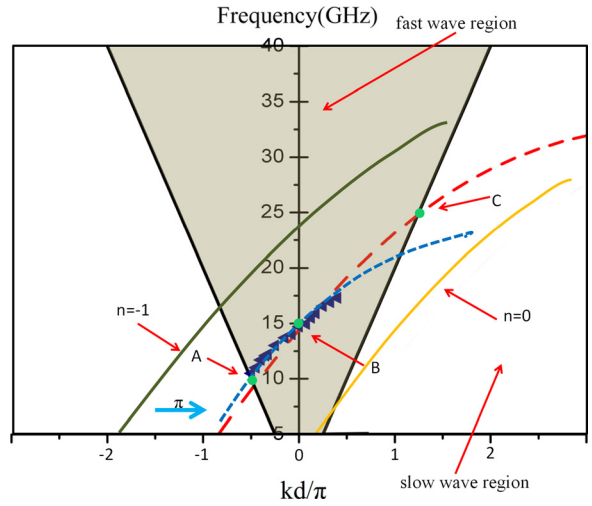

FIG. 3. The Brillouin diagram (vs. frequency) for the n = −1 space radiating harmonic obtained for the structure with period $l = 11.1$ mm and $g = 6$ mm. The shaded area represents the fast-wave region, and the black solid lines represent the light lines. The dispersion curve for the corresponding unit cell without phase reversals (orange solid curve (n = 0)) is also shown for reference. The green solid curve (n = −1) for the case of a leftward (180 phase advance) shift is represented by a red dashed curve, which is almost coincident to the blue dashed curve extracted by the angle solutions (2) (blue dashed curve fitted by dots of the triangle).

layers ranges from 6 mm to 0, it will result in gradual deviation of the dispersion curves from the light line. We notice that the dispersion curve of the double-strip structure deviates more than that of the single-strip structure, which implies that the double strips can confine the EM fields more tightly and enhance the EM fields more significantly around the structure simultaneously.

The surface mode is mainly confined at the interface, and the electric boundaries of localized surface fields would be destroyed when the phase-reversal geometry is introduced. In this case, the phase-reversal structure generates the desired periodic modulation of the electric field, and the space harmonics are excited around the perturbations. According to the Bloch–Floquet theorem,[30–33] an infinite number of space harmonics are generated automatically by the periodic modulation in which the phase constant β_n of the nth harmonic is given by:

$$\beta_n(w) = \left[\beta_0(w) \pm \frac{2\pi n}{p}\right], \quad n = 0, \pm 1, \pm 2..., \tag{1}$$

where β_0 is the phase constant of the n = 0 space harmonic and p is the period of the structure. β_n is simply a repetition of β_0 with a period of 2π, and the physical functions that depend on the dispersion relation will merely repeat themselves periodically outside the first Brillouin zone. The phase-reversal structure of adjacent elements introduces a frequency-independent 180° phase shift per unit cell from the point of view of the radiation field. The resulting dispersion characteristics are shown to be the 180° phase shift horizontally from the original dispersion curve. Consequently, the $n = -1$ spatial harmonic is located inside the first Brillouin zone. In Figure 3, the gray region indicates the fast-wave (radiating) region, and the yellow solid line and the green solid line represent the $n = 0$ and $n = -1$ space harmonics, respectively, whereas the red dashed line represents the 180° phase shift horizontally (rightward) from the original dispersion curve ($n = -1$).

The radiation characteristics of the periodic coupling structure can be analyzed by using the concept of diffraction radiation. When a charged particle with charge q moves along the x axis with a constant velocity v, an equivalent current density is generated, which is given by

$$\bar{J}_p(x, y, z, t) = \hat{x} q v \frac{\delta(\rho)}{2\pi\rho} \delta(x - vt), \tag{2}$$

where ρ represents the radial dimension in the y-z plane, δ is the Dirac delta function, and t is the time. Through the use of Fourier transform, we obtain the expression of this current in the frequency domain as

$$\bar{J}_p(x, y, x, w) = \hat{x} q \frac{\delta(\rho)}{4\pi^2\rho} e^{ik_x x}, \tag{3}$$

where w is the frequency and $k_x = \frac{w}{v}$ is the wave vector along the x axis. We use a dipole array to model the phase-reversal geometry. Each dipole has a current with amplitude I, a period length l, and a phase shift $k_x l$ relative to its adjacent element. The current density of the dipole array is the sum of the current densities of all the dipoles

$$\begin{aligned} \bar{J}_d(x, y, z, t) &= \hat{x} \frac{Il\delta(\rho)}{2\pi\rho} \sum_{n=-\infty}^{\infty} \delta(x - nj) e^{ink_x l - iw_0 t}, \\ &= \hat{x} \frac{I\delta(w - w_0)}{2\pi\rho} \delta(\rho) e^{ik_x x}. \end{aligned} \tag{4}$$

The interaction mechanism for radiations can be obtained by a rigorous dispersion analysis. Cherenkov radiation occurs under the angle

$$\theta_c(w) = \sin^{-1}[c/nv_p)] = \sin^{-1}[c\beta(w)/w], \quad k_x = \beta(w) - j\alpha, \tag{5}$$

where v_p is the wave velocity in the medium and $\beta(\omega)$ is the corresponding phase constant. Thus, β can be predicted by the measured angle θ_c. It can be seen that the beam scans nearly from the backward to forward (between points A and C in Fig. 3) as the frequency increases. The blue dashed line

identifies the dispersion curve extracted by the angle solution (2), whereas the red dashed line represents the phase shift π from the original dispersion curve ($n=-1$). Both curves have a similar slope distribution, and the value of β/k_0 changes with the frequency.

In order to get more physical insights on the study of mode conversion during the transition, we simulate the cross-section electric field distributions. A comparison between the spoof SP waveguides with (see Fig. 4(a)) and without the phase-reversal structure (see Fig. 4(b)) is illustrated in Figure 4. We notice that the distribution of the E-field vector is mainly concentrated in the gaps between the upper and lower layers of the waveguide when without the phase-reversal structure, as illustrated in Fig. 4(a).

The E-field vector distribution is clearly no longer confined near the groove when introducing the periodic phase-reversal structure, as demonstrated in Fig. 4(b). The new structure alters the direction of the E-field vector between the upper and lower strips, which is mainly along the Y direction. As a result, the radiation mode is excited by the transverse E-field E_y, which is leaked via the minor impedance discontinuities.

To facilitate the excitation of SP modes by guided waves, a tapered structure for multistage transition is added at both ends of the double-layer corrugated strips[26] in which the groove depth h progressively increased from 0.4 mm to 1.2 mm to achieve a good matching of both momentum and impedance. The overall 10-cell antenna, including the transitions and connection stripline, is about 190 mm long. The periodicity adds a degree of freedom in the design of radiation properties. We fabricated samples and measured their transmission and reflection properties. It is obvious that in a wide frequency range of 12–16.2 GHz, the reflection coefficient (S11 or S22) is less than −10 dB, whereas the transmission coefficient (S21) is less than −30 dB. That is to say, only few waves are reflected back to the feeding point or transmitted to the other port. Meanwhile, the open stopband is effectively suppressed around the broadside (point B, about 15.1 GHz).[34,35] Furthermore, the distribution of aperture-field amplitude (or the directivity) is primarily controlled by the attenuation coefficient α, which can be extracted by the equation: $\alpha = -\frac{\ln(|S_{11}|^2+|S_{21}|^2)}{2L_a}$, as illustrated in Figs. 6(b) and 6(c).

Further studies reveal the following radiation characteristics. To have the direct understanding of the symmetric Cherenkov radiation wakes, we set an area at the cross section (i.e., the XOY plane) parallel to the propagation direction to observe the electric field. Figure 5 shows the numerical simulation results of the near-field intensity distributions (the absolute value) at different frequencies (12.0, 12.8, 15.0, and 15.7 GHz, respectively). When the wave-propagation velocity is faster than the phase velocity in the dielectric medium, this decay constitutes a Cherenkov radiation effect. It can be observed from the figure that the surface wave is coupled to the radiation mode and then leaked into the space. Meanwhile, it is a leaky mode and its beam may be steered by tuning the frequency. The main beam angle is primarily determined by the phase constant β. The measurement results are in excellent agreement with the theoretically expected angles given by Eq. (2), as illustrated in Fig. 6(a). In addition, we also note that an analogue to the reversed Cherenkov radiation wakes occurs at 15.7 GHz since the radiation in the forward or backward direction is relative to the phase constant β, as shown in Fig. 5(d), which was previously observed in the negative-index metamaterials.[6]

In summary, we proposed a tunable SP radiation source based on the diffraction radiation mechanism. The phase-reversal structure causes an extra phase shift between adjacent unit cells, which results in a horizontal shifting of the entire dispersion diagram by an amount of π. The radiation mechanism is explained in terms of introducing a harmonic wave by periodic loading of the phase-reversal structure. Furthermore, each period generates an independent plasmon wavefront, and the phenomenon of Cherenkov radiation wakes was experimentally demonstrated, including the reversed Cherenkov radiation wakes that were originally observed in the negative-index metamaterials. In particular, the structure might be applied effectively for the elimination of the open stopband at broadside. This technique could be

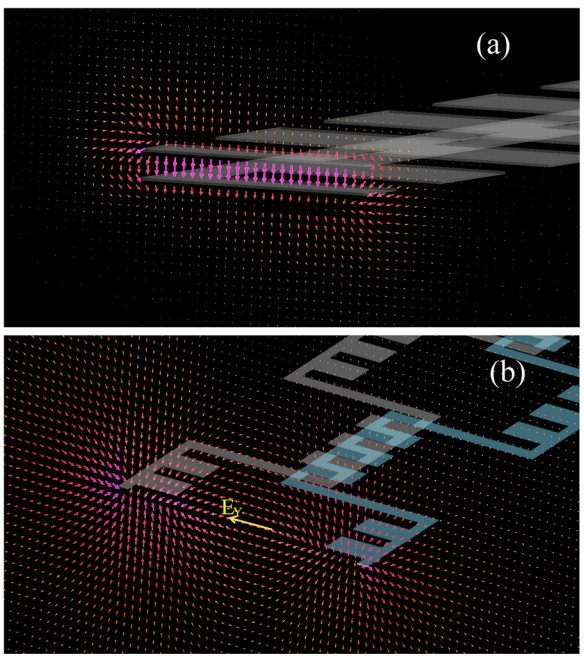

FIG. 4. The cross-section E-field vector distributions at the junction for spoof SP waveguides with (a) and without (b) the phase-reversal structure.

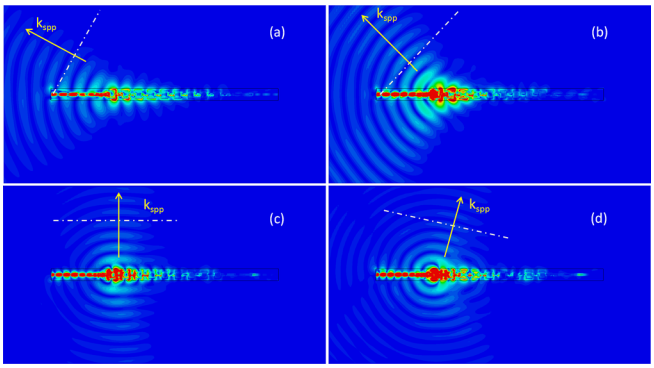

FIG. 5. (a)–(d) The numerical simulation results of the near-field intensity distributions (the absolute values) at different frequencies (12.0, 12.8, 15.0, and 15.7 GHz, respectively).

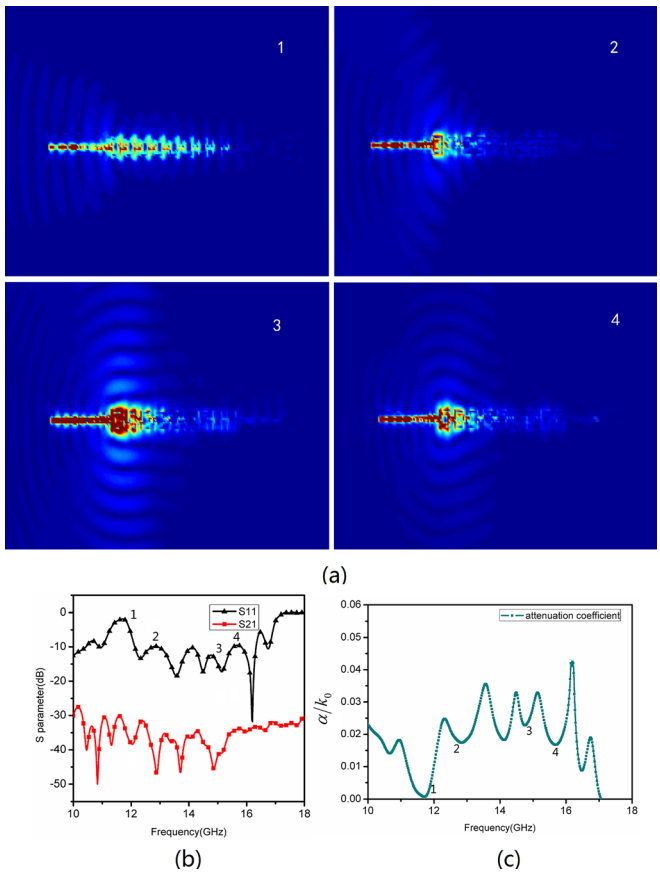

FIG. 6. (a) The experimental results of the near-field intensity distributions (the absolute values) at different frequencies (12.0, 12.8, 15.0, and 15.7 GHz, respectively). (b) The measured reflection and transmission coefficients (S-parameters). (c) The attenuation constant normalized to the free-space wave number. The numbers marked on the figure correspond to the frequencies, respectively.

an alternative to transforming the SP waves into radiation waves.

This work was supported in part by the National Science Foundation of China under Grant Nos. 61631007, 61571117, 61501112, 61302018, 61401089, and 61501117 and in part by the 111 Project under Grant No. 111-2-05.

[1]V. V. Vorobev and A. V. Tyukhtin, Phys. Rev. Lett. **108**, 184801 (2012).
[2]P. Zhang, M. Hu, R. B. Zhong, X. X. Cheng, S. Gong, T. Zhao, and S. G. Liu, J. Phys. D: Appl. Phys. **49**, 145302 (2016).
[3]V. Ginis, J. Danckaert, I. Veretennicoff, and P. Tassin, Phys. Rev. Lett. **113**, 167402 (2014).
[4]M. I. Bakunov, A. V. Maslov, and S. B. Bodrov, Phys. Rev. B **72**, 195336 (2005).
[5]X. Shi, X. Lin, F. Gao, H. Xu, Z. Yang, and B. Zhang, Phys. Rev. B **92**, 081404(R) (2015).
[6]S. Xi, H. S. Chen, T. Jiang, L. X. Ran, J. T. Huangfu, B. I. Wu, J. A. Kong, and M. Chen, Phys. Rev. Lett. **103**, 194801 (2009).
[7]S. Liu, P. Zhang, W. Liu, S. Gong, R. Zhong, Y. Zhang, and M. Hu, Phys. Rev. Lett. **109**, 153902 (2012).
[8]M. I. Bakunov, E. A. Mashkovich, and E. V. Svinkina, Opt. Lett. **39**, 6779 (2014).
[9]P. Genevet, D. Wintz, A. Ambrosio, A. She, R. Blanchard, and F. Capasso, Nat. Nanotechnol. **10**, 804 (2015).
[10]A. Bera, R. K. Barik, M. Sattorov, O. Kwon, S. H. Min, I. K. Beak, S. Kim, J. K. So, and G. S. Park, Opt. Express **22**, 3039 (2014).
[11]J. K. So, J. H. Won, M. A. Sattorov, S. H. Bak, K. H. Jang, G. S. Park, D. S. Kim, and F. J. Garcia-Vidal, Appl. Phys. Lett. **97**, 151107 (2010).
[12]P. Kumar, L. Bhasin, V. K. Tripathi, A. Kumar, and M. Kumar, Phys. Plasmas **23**, 093301 (2016).
[13]S. Liu, M. Hu, Y. Zhang, Y. Li, and R. Zhong, Phys. Rev. E **80**, 036602 (2009).
[14]S. Gong, M. Hu, R. B. Zhong, X. X. Cheng, T. Zhao, and S. G. Liu, Opt. Express **22**, 19252 (2014).
[15]H. Saito, S. Mizuma, and N. Yamamoto, Nano Lett. **15**, 6789 (2015).
[16]X. Shen and T. J. Cui, Appl. Phys. Lett. **102**, 211909 (2013).
[17]H. F. Ma, X. Shen, Q. Cheng, W. X. Jiang, and T. J. Cui, Laser Photonics Rev. **8**, 146 (2014).
[18]S. L. Sun, Q. He, S. Y. Xiao, Q. Xu, X. Li, and L. Zhou, Nat. Mater. **11**, 426 (2012).
[19]L. B. Kong, C. P. Huang, C. H. Du, P. K. Liu, and X. G. Yin, Sci. Rep. **5**, 08772 (2015).
[20]J. J. Xu, H. C. Zhang, Q. Zhang, and T. J. Cui, Appl. Phys. Lett. **106**, 021102 (2015).
[21]N. Yu, P. Genevet, M. A. Kats, F. Aieta, J. P. Tetienne, F. Capasso, and Z. Gaburro, Science **334**, 333 (2011).
[22]W. Ni, X. S. Kou, Z. Yang, and J. F. Wang, ACS Nano **2**, 677 (2008).
[23]D. O'Connor, P. Ginzburg, F. J. Rodríuez-Fortuñ, G. A. Wurtz, and A. V. Zayats, Nat. Commun. **5**, 5327 (2014).
[24]A. V. Shchegrov, I. V. Novikov, and A. A. Maradudin, Phys. Rev. Lett. **79**, 2597 (1997).
[25]Z. H. Han and S. I. Bozhevolnyi, Rep. Prog. Phys. **76**, 016402 (2013).
[26]H. C. Zhang, S. Liu, X. Shen, L. H. Chen, L. Li, and T. J. Cui, Laser Photonics Rev. **9**, 83 (2015).
[27]H. C. Zhang, T. J. Cui, Q. Zhang, Y. Fan, and X. Fu, ACS Photonics **2**, 1333 (2015).
[28]Z. L. Ma, L. J. Jiang, S. Gupta, and W. E. I. Sha, IEEE T. Antennas Propag. **63**, 113 (2015).
[29]N. Yang, C. Caloz, and K. Wu, IEEE Trans. Microwave Theory **58**, 2619 (2010).
[30]F. Monticone and A. Alu, Proc. IEEE **103**, 793 (2015).
[31]V. A. Kostin and N. V. Vvedenskii, New J. Phys. **17**, 033029 (2015).
[32]S. Otto, A. Rennings, K. Solbach, and C. Caloz, IEEE Trans. Antennas Propag. **59**, 3695 (2011).
[33]K. Kaasbjerg and A. Nitzan, Phys. Rev. Lett. **114**, 126803 (2015).
[34]J. T. Williams, P. Baccarelli, S. Paulotto, and D. R. Jackson, IEEE Trans. Antennas Propag. **61**, 4484 (2013).
[35]S. Otto, A. Al-Bassam, A. Rennings, K. Solbach, and C. Caloz, IEEE Trans. Antennas Propag. **62**, 5037 (2014).